Jurnal Teknologi

Full Paper

BUILDING INTER-STOREY DRIFT UNDER CONSISTENT PSEUDO DYNAMIC LOAD

Weng Khuen Chong[a], Chun-Chieh Yip[a]*, Lloyd Ling[a], Jing-Ying Wong[b], Foong-Sin Lam[a], Yen-Sin Lim[a]

[a]Department of Civil Engineering, Universiti Tunku Abdul Rahman, Bandar Sungai Long, 43000, Cheras, Kajang, Selangor, Malaysia
[b]Department of Civil Engineering, University of Nottingham Malaysia, Semenyih 43500, Selangor, Malaysia

Article history
Received
4 November 2024
Received in revised form
27 February 2025
Accepted
18 March 2025
Published Online
23 December 2025

*Corresponding author
yipcc@utar.edu.my

Graphical abstract

Abstract

Earthquakes are among the most destructive natural disasters, causing widespread fatalities and destruction globally. This research investigates the inter-storey drift performance and mode shape of a 1:8 downscaled model of a 1-bay, 3-storey reinforced concrete model (DRCM), constructed based on a high school building's perimeter skeleton for dynamic load testing with the assistance of Similitude Theory and Buckingham's Pi Theorem. By addressing the research gaps, consistent ground accelerations are considered rather than existing seismic data from past earthquakes by utilising a shaking table (ST) to simulate ground motion and test the DRCM. The findings indicate that inter-storey drift increases significantly with large, low-aggressiveness ground movements, while higher earthquake intensity results in reduced structural movement characterised by intense vibrations. The structure transitions from a single curvature to a double curvature mode of oscillation under increasing ground acceleration. Testing three brands of viscous dampers revealed that they effectively reduce inter-storey drift, with rooftop displacements decreased by 45%, 63%, and 34% for the APIDO, SKK, and ESPADA dampers, respectively. Finding shows damper with the highest damping constant (APIDO) excels in absorbing large displacements, whereas the least viscous force damper (SKK) is better suited for mitigating lateral displacements during intense vibrations.

Keywords: Earthquake, Seismic Resistance, Viscous Dampers, Inter-Storey Drift, Downscaled Reinforce Concrete Model

Abstrak

Gempa bumi adalah antara bencana alam yang paling merosakkan, menyebabkan kehilangan nyawa dan kemusnahan yang meluas di seluruh dunia. Penyelidikan ini menyiasat prestasi susut antara tingkat dan bentuk mod bagi model konkrit bertetulang berskala 1:8 (DRCM) dengan 1 petak dan 3 tingkat, yang dibina berdasarkan rangka perimeter bangunan sekolah menengah untuk ujian beban dinamik dengan bantuan Teori Keserupaan dan Teorem Pi Buckingham. Dengan menangani jurang penyelidikan, pecutan tanah yang konsisten dipertimbangkan berbanding data seismik sedia ada dari gempa bumi lepas dengan menggunakan meja gegaran (ST) untuk mensimulasikan gerakan tanah dan menguji DRCM. Dapatan kajian menunjukkan bahawa susut antara tingkat meningkat dengan ketara dengan gerakan tanah yang besar dan rendah agresif, manakala intensiti gempa bumi yang lebih tinggi mengurangkan pergerakan struktur yang dicirikan oleh getaran yang kuat. Struktur tersebut beralih daripada bentuk

mod lengkung tunggal kepada lengkung berganda apabila pecutan tanah meningkat. Ujian ke atas tiga jenama peredam likat mendedahkan bahawa kesemuanya berkesan mengurangkan susut antara tingkat, dengan pengurangan anjakan bumbung sebanyak 45%, 63%, dan 34% masing-masing untuk peredam APIDO, SKK, dan ESPADA. Peredam dengan pemalar redaman tertinggi (APIDO) terbukti cemerlang dalam menyerap anjakan besar, manakala peredam dengan daya likat paling rendah (SKK) lebih sesuai untuk mengurangkan anjakan lateral semasa getaran yang kuat.

Kata kunci: Gempa Bumi, Ketahanan Seismik, Damper Viskos, Anjakan Antara Tingkat, Model Konkrit Bertetulang Skala

1.0 INTRODUCTION

Earthquakes are among the most destructive natural disasters in human history, resulting in the deaths of hundreds of thousands of people and the destruction of property worth billions of dollars. While the global death toll from natural disasters is lower today than in historical times, thanks to increased adaptability, but earthquakes still claim a significant number of lives each year. Earthquakes can also trigger secondary hazards, such as surface fractures, landslides, liquefaction, and tsunamis [1, 2].

The deadliest earthquake in recorded history occurred in Shaanxi, China, on January 23, 1556, with a magnitude of 8. It resulted in approximately 830,000 deaths. Although the earthquake lasted only a few seconds, it toppled mountains, shifted the course of rivers, created cracks up to 20 meters deep, and caused major landslides, along with devastating floods and fires that lasted for days [3]. Over 60% of the population perished, as most homes were built using soft soil with no seismic resilience. When the earthquake struck, these homes collapsed, and entire hillsides slid, burying entire communities [4].

In contrast, Malaysia, located on the Sunda Plate within the Eurasian Plate and surrounded by the Philippine Plate and Indian-Australian Plate [5,6], is considered a region with low seismic activity. However, regional earthquakes caused by Sumatra's fault lines and subduction zones do affect Malaysia. Additionally, the eastward movement of the Sunda Plate at a rate of 10 cm/year relative to the Eurasian Plate contributes to local earthquakes in Malaysia [7]. East Malaysia, particularly Sabah and Sarawak, is more prone to earthquakes due to its proximity to these tectonic plates [8]. The interaction and movement of the major tectonic plates in Southeast Asia toward Malaysia cause subduction zones and near-field earthquakes, as shown in

Figure **1** [5]. According to records from the United States Geological Survey (USGS) and the European-Mediterranean Seismological Centre (EMSC), Malaysia has experienced 218 earthquakes with magnitudes of 4.0 or higher within a 300 km radius. Earthquakes with a magnitude of 4.0 can often be felt up to 400 km away from the epicenter, though it rarely cause significant damage near the source [5,9].

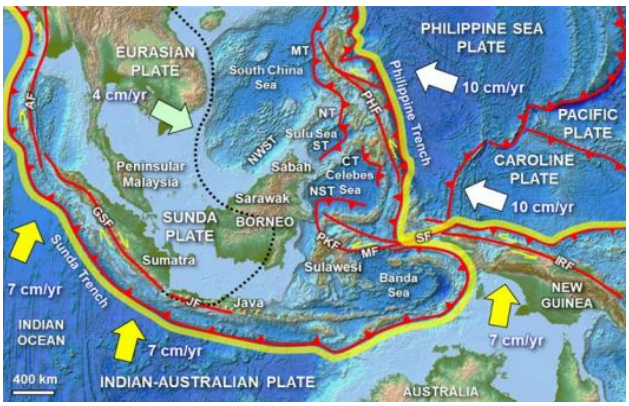

Figure 1 Plate tectonic margins and movements in Southeast Asia. [5]

In 2023, the chief researcher from Universiti Teknologi Malaysia (UTM) Seismology and Earthquake Engineering Research Group, Prof. Ir. Dr. Azlan Adnan, emphasized the need for Malaysians to enhance their preparedness for potential earthquakes, as the country is no longer outside the Pacific Ring of Fire [10]. As a result, seismic performance must be improved in structural designs to minimize earthquake responses and ultimately reduce the devastating impacts of earthquakes.

One of the concepts of mitigating the economic loss from earthquakes for low-rise buildings is to implement a seismic damper system between structural members [11, 12]. This is due to seismic damper enabled to reduce kinetic energy delivered to the structure by converting seismic energy to heat energy by moving the compressible fluid contained within the viscous dampers [13,14]. Also, several researchers proven that seismic damper systems can enhance the seismic performance of existing buildings with and without seismic damper [15–17]. However, past research has revealed a significant gap in experiments involving downscaled reinforced concrete (RC) buildings with and without dampers.

Furthermore, earlier research relied on seismic ground movements derived from historical earthquakes, which earthquakes are produced by seismic events in a dynamic environment, and every earthquake is different [18]. Hence, current research uses a variety of constantly dynamic ground movements up to 3.15g, which corresponds to a return time of 4,000 years in NYC and 25,000 years in San Francisco, CA. The 3.15g ground movements are chosen as a suitable reference probability in building design via load combinations, according to the US Nuclear Regulatory Commission, guaranteeing that vital services buildings can resist earthquakes [19].

Experimental testing is crucial for advancing technology and validating new approaches in structural engineering [20]. Since full-scale structural testing is complex, costly, and time-consuming, small-scale models are often used in laboratory experiments. However, even with perfect scaling, these models can exhibit different ultimate capacities compared to their full-scale counterparts, meaning their static and dynamic responses may not entirely align [21]. To address this, similitude theory is applied to ensure similarity between the model and the full-scale prototype. When similitude conditions are met, the model is expected to behave like the prototype, and the results obtained from the scaled model can be used to predict the structural response of the full-scale version [21–24].

Buckingham's Pi theorem is often used alongside similitude theory. This theorem reduces the number of parameters involved in the system by identifying dimensionless groups, with the most common fundamental dimensions being length (L), time (T), and either mass (M) or force (F) [25]. According to the theorem, the equation must remain consistent regardless of the units involved in the physical variables [21]. A scale factor, S, is applied in each equation to account for the differences between the prototype and the scaled model, ensuring that similitude conditions are met. The scale factor is particularly important for scaling linear dimensions, including height, width, length, and thickness. Table 1 shows the summary of the basic parameter for an elastic model.

Table 1 Summary of basic parameter for an elastic model [21–24]

Parameter	Scale Factor
Dimension	S
Area A_p	S^2
Volume V_p	S^3
Linear displacement U_p	S
Moment of inertia I_p	S^4
Frequency f	$S^{-1/2}$ or $(S/S_a)^{-1/2}$
Time	$(S/S_a)^{1/2}$
Density ρ_p	S_e/S^aS
Point load F_p	S_eS^2
Line load F_L	S_eS
Uniform distributed load P_p	S_e
Shear force V_p	S_eS^2

The shaking table assessment (STA) is one of the most widely used techniques for investigating the dynamic behaviour of structures in earthquake engineering [26]. The mechanical performance of bracing systems in structures can be assessed using a scaled model in a STA [27]. Currently, the STA is the only experimental method capable of simulating real earthquake loadings in a laboratory setting [28]. Through this test, both steady-state and random shaking can be simulated, generating different wave motions. A harmonic wave is used for steady-state shaking, while a random wave of white noise is employed for random shaking. Low-amplitude harmonic waves allow the test model to remain within its elastic range, enabling the study of its dynamic properties.

This study built upon previous research [17] and specifically addressed existing gap by removing the damper springs or known as backbone curve to investigate the inter-storey drift performance of a scaled reinforced concrete building without and with three various types of dampers. The selection of three different types of dampers aimed to assess their effectiveness in mitigating seismic-induced inter-storey drift at varying viscosities, ultimately identifying the most suitable damper type for specific seismic scenarios. A 1:8 downscaled, single-bay, three-story reinforced concrete model (DRCM) has been constructed for STAs in the laboratory. The significance of this research is to provide guidance and reference for improving the displacement response and seismic resistance of structures during earthquakes as three-story residential property remains the major favour of property type in Malaysia according to Malaysia Property Market Centre (NAPIC). The study of energy dissipation devices offers consulting firms an additional option when designing structures to account for lateral loads, including seismic loading. Furthermore, this research addresses the gap of using consistent ground accelerations rather than existing seismic data from past earthquakes by utilizing a shaking table (ST) to simulate ground motion and test the DRCM.

2.0 METHODOLOGY

2.1 DRCM Specification

Figure 2 shows the geometry and specifications of the 1:8 downscaled, single-bay, three-story DRCM based on a high school building prototype. The total height of the DRCM is 1.5 m, with each storey measuring 0.5 m. The footings, which are bolted to the ST, have dimensions of 175 mm in width and length, with a footing depth of 50 mm. The scaled beam has dimensions of 31 mm in width and 75 mm in depth. The columns are square, with dimensions of 40 mm. The slab is scaled to a thickness of 16 mm, with a width and length of 830 mm for the entire DRCM. Based on these dimensions, the total volume of concrete in the DRCM is approximately 0.072 m³, equivalent to a mass of around 170 kg.

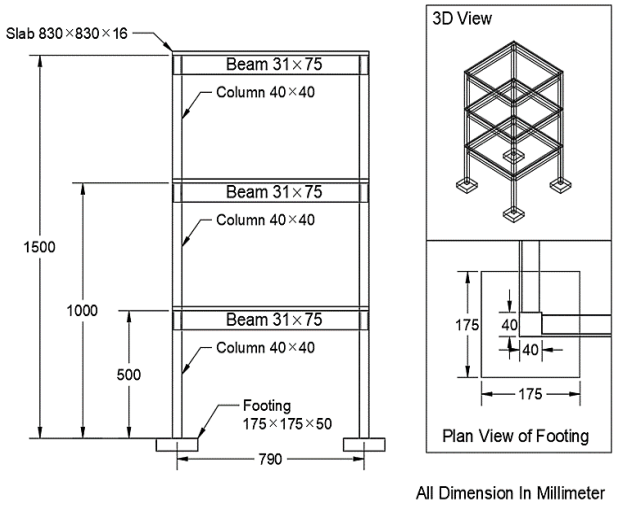

Figure 2 DRCM geometry

Since the ST used in this study is capable of supporting up to 3000 kg, the test can be conducted with this DRCM. Additionally, the DRCM can be placed on the ST, as there is a 2.5 m height clearance available. Due to the relatively small dimensions of the structural members, 3 mm steel bars were used as the main reinforcement, while 1 mm steel wires were used for shear reinforcement.

2.2 Concrete Mix Specification

The self-compacting concrete was designed to achieve a compressive strength of 30 N/mm² at 28 days. The mix proportions of the raw materials for producing 1 m³ of concrete were based on the experiment conducted by Yip *et al*. [17,21,22], following British Standard BS5328: Part 2: 1997, as shown in Table 2. The resulting concrete had a density of 2380 kg/m³, and the water-to-cement ratio was 0.42, which is relatively low. To improve the workability of the mix, a superplasticizer was added in a small dosage, equal to 1.2% of the concrete weight. The coarse aggregate, commonly known as pebble stone, was selected in a rounded shape and downscaled from 21mm to 3mm using the similitude law. Meanwhile, river sand was chosen as the fine aggregate, retaining a 0.075mm sieve size to enhance the flowability and passing ability of the DRCM.

Table 2 Mix proportions of concrete with characteristic strength of 30 N/mm² [17,21,22]

Water/cement ratio	0.42
Cement (kg/m³)	550.0
Water (kg/m³)	233.0
Fine aggregate (kg/m³)	511.0
Coarse aggregate (kg/m³)	1086.0
Density (kg/m³)	2380.0
Admixture 1.2 % (kg)	6.6

Table 3 shows the findings of concrete compressive test that carried out according to the ASTM C39 [29,30] standard. Since the concrete used in the DRCM was grade C30, the characteristic strength of the concrete was designed to be 30 MPa. At 14 days, the concrete was expected to achieve around 90% of its final strength, meaning the target strength for the concrete cylinders was set at 27 MPa. The results indicated that the compressive strength of the cylinder specimens was sufficient, confirming that the mix proportions were satisfactory. This concrete mix was subsequently used in constructing the DRCM for this study.

Table 3 Compressive strength of 3 concrete cylinders

Concrete specimen	1	2	3
Ultimate load, P (kN)	224.8	216.6	213.3
Compressive strength (MPa)	28.62	27.58	27.16
14th day ideal strength (MPa)	27	27	27
Status	Pass	Pass	Pass

2.3 Casting of DRCM

Figure 3 shows the reinforcement preparation, casting process, and completed single-bay, three-story DRCM. The timber plywood formwork was wrapped in a layer of plastic to enhance its water resistance and facilitate easier dismantling. Steel bars measuring 3 mm in diameter were cut to suitable lengths and bent into the required shapes for the main reinforcement of the structural members, while 1 mm steel wires were used as stirrups for the shear reinforcement. The reinforcement for the footings, along with the column starter bars, was placed into the footing formwork, and the concrete was cast. After 24 hours, the footing formwork was dismantled, and the footings were inspected to ensure that no honeycombing had occurred, which could weaken the concrete strength.

Construction of the DRCM continued with the casting of the columns, beams, and slab for the first floor. After casting the columns, the top surfaces were smoothed using a grinder to provide an even surface for the beam casting. The beams and floor slab were cast simultaneously to simplify the construction process. This casting procedure was repeated for the second and third floors. The DRCM was cured by spraying water on the concrete surface for seven days after each casting to maintain adequate moisture levels. Once all the structural elements were cast, the DRCM was painted and left to cure for 28 days before the STA.

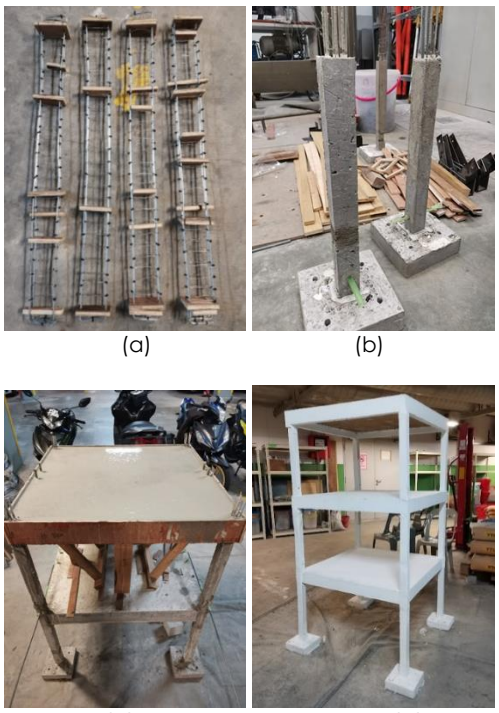

(a) (b) (c) (d)

Figure 3 Photo gallery of (a) Rebar work; (b) Column demould; (c) Slab casting; (d) Complete DRCM

2.4 Experimental Test Set-up

Figure 4 shows the uniaxial ST used to simulate seismic movements in this research. The ST is powered by a direct-drive motor, also known as a torque motor. When the frequency and displacement of the shaking are input into the computer, the actuator generates linear movements according to the input, replicating the ground-shaking motions experienced during earthquakes. This ST can simulate movement within a frequency range of 0.1 Hz to 20 Hz and a displacement range from 0.5 mm to 15 mm.

Figure 4 Shaking Table

LVDT (Linear Variable Differential Transformer) displacement sensors recorded the inter-storey drift, displacement, movement, and sway distance of the DRCM during the STA. Two 25 mm LVDTs were installed on the first floor of the DRCM and on the ST, representing the ground floor, while two 50 mm LVDTs were installed on the second and third floors. A data logger recorded the real-time displacement data of the DRCM. Table 4 provides information about two models of LVDT displacement sensors (KA-SA-020 and KA-SA-030), both featuring a ±10V output but differing stroke ranges of ±20 mm and ±30 mm, respectively. Both sensors are from KYOWA (Japan) and operate safely within a temperature range of -10°C to +80°C, with temperature coefficients of 100 ppm/°C and 50 ppm/°C.

Table 4 Specification of LVDT displacement sensor

Model	KA-SA-020	KA-SA-030
Output / Stroke	±10V / ±20 mm	±10V / ±30 mm
Temperature Coefficient	±100 ppm/°C	±50 ppm/°C
Brand / Origin	KYOWA, Japan	
Safe Temperature	-10 ~ +80°C	

The procedure for conducting the STA begins with the end user inputting the gear displacement (in mm) and frequency (in Hz) into the motor-controlling software. The inputted signals are then sent to the motor, preparing it for shaking based on the combined effects of the input parameters.

To ensure accurate and consistent raw data collection, it is crucial to properly position the LVDT displacement sensors and accelerometers. This recording equipment was connected to a data logger, which transfers and converts the analogue signals into digital format. The data logger used in this study is the TML DRA-30A from Tokyo Measuring Instruments Laboratory Co., Tokyo, Japan. This logger can simultaneously receive data from 30 channels, and its specifications shown in Table 5, with a maximum data memory capacity of 112,000 words per channel at 5 milliseconds.

Table 5 Specification of data logger model TML DRA-30A

Strain	
No. of channels:	30
Quarter bridge in 3 wires:	120Ω
Half bridge:	120Ω~1000Ω
Full bridge:	120Ω~1000Ω
Gauge factor:	2.00 fixed
Bridge excitation:	2V DC
Initial value memory:	±10000 × 10^{-6} strain
Measuring range:	±20000 × 10^{-6} strain
Accuracy	
Static in full bridge:	±0.2% reading + 3 digit
Dynamic:	±0.2% reading + 5 digit
Resolution:	1 × 10^{-6} strain
Static:	±0.2% reading + 3 digit
Dynamic:	±0.2% reading + 5 digit
Resolution:	1mV
On zero:	±2 × 10^{-6} strain/°C or less (Dynamic)

The end user was allowed to input acceptable gear displacement and frequency values, but with specific limitations. For optimal STA operation, each input must be either one high displacement with one low frequency, or one low displacement with one high frequency, and vice versa. Thus, it was necessary to study and identify the idealized realistic input combinations for the STA to achieve output results that closely resemble real-time earthquake data.

Figure 5 shows three brands of viscous dampers tested to compare their performance under different SLs of earthquake simulation. The length of the cylinder containing compressible fluid for each damper is varied, while the total length of each damper is constant.

(a) (b) (c)

Figure 5 (a) Damper 1 (Apido); (b) Damper 2 (Espada); (c) Damper 3 (SKK)

Figure 6 shows the setup of the DRCM with an inverted V diagonal braced-damper system for the STA.

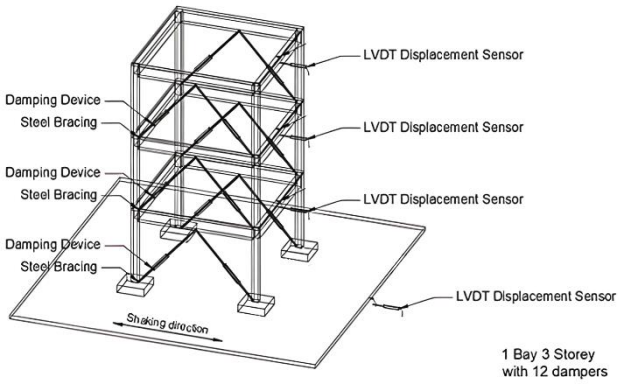

Figure 6 Experimental set-up of DRCM with dampers

The inverted V diagonal braced-damper system was chosen to enhance energy dissipation in both positive and negative directions, ensuring balanced load distribution between the two diagonal members and reducing unbalanced moments on the beams and columns [31]. To operate the ST, a 420V alternating current had to be transformed into 200V. In addition to the STM, the setup included accompanying software and recording equipment for data acquisition. This equipment comprised signal controllers, device-control software, motor-control software. Each floor was installed one LVDT displacement sensor for recording the seismic response. In addition, structural damage mechanisms were closely observed throughout the test, with any cracking marked and recorded after each seismic level (SL) of earthquake simulation.

3.0 RESULTS AND DISCUSSION

3.1 Earthquake Simulations

Table 6 presents the displacement and aggressiveness of each SL of STA conducted in this study. A total of ten SLs of earthquake simulations were carried out randomly, without predetermining the peak ground acceleration. The intensity of the earthquake simulation increases when the shaking is more aggressive, accompanied by shorter displacement. As the shaking SL rises, the shaking frequency generally increases while the unit displacement decreases.

Table 6 Intensity of each SL of earthquake simulation

SL	ST Inputs		ST Outputs		
	χ (mm)	f (Hz)	χ_{ground} (mm)	a_{ground} (m/s^2)	G-force (g)
1	3	1	18.23	7.26	0.74
2	3	2	18.26	16.58	1.69
3	1.5	3	10.91	19.13	1.95
4	1.9	3	12.69	18.05	1.84
5	1	5	7.45	13.64	1.39
6	0.7	7	3.57	13.93	1.42
7	0.6	8	3.05	16.97	1.73
8	0.6	10	3.10	22.46	2.29
9	0.3	15	1.02	23.64	2.41
10	0.5	15	1.98	30.90	3.15

SL1 and SL2 categorized as low frequency waves, but waves from SL2 with moderate motion. SL3 and SL4 classed as low-to-moderate frequency waves, whereby SL3 with faster motion when compared to SL4. SL5 was a medium frequency waves that have moderate intensity. Based on the ST inputs, SL1 to SL5 were known as surface or primary waves (P-waves) that represented far field seismic events from Sumatra and Philippine trenches, which Malaysia frequently experiences. Damage of P-waves mostly observe on buildings region such as Kuala Lumpur and Pulau Pinang, Malaysia.

Moreover, SL6 to SL8 were sorted as high frequency waves or known as secondary waves (S-waves) and sharp seismic waves. S-waves represented near field tremors from local faults such as 2015 Ranau, Sabah earthquake. The S-waves

significantly damage to low rise structures due to rapid oscillations. Therefore, the study of S-waves was important as almost 70% of residential houses in Malaysia fall under the landed property category according to NAPIC.

In addition, SL9 and SL10 were categorized as very high-aggressiveness waves. The waves do not typically experience in Malaysia but is crucial for research purposes and modelling worst case scenarios for enhanced structural readiness. In short of design parameters, the relationship between the displacement response of the DRCM can be observed. Each assessment of pseudo-dynamic load testing lasted for 15 seconds to collect the displacement response of the DRCM.

Figure 7 shows the 15 seconds ST ground acceleration output for SL 1, with a peak value of 7.26m/s^2.

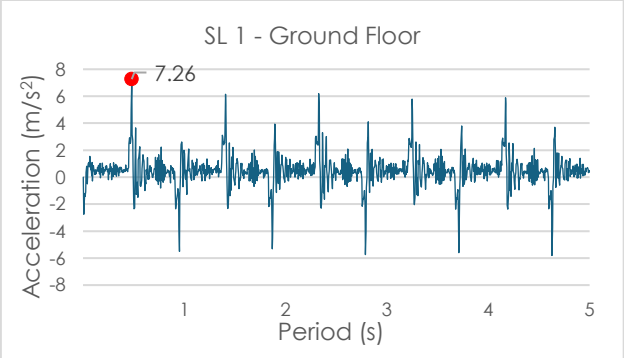

Figure 7 ST ground acceleration output at SL1

3.2 Viscous Damping Constant of All Dampers

The mechanical properties of viscous dampers were tested using a Universal Tensile Machine (UTM) to determine the damping coefficient from the hysteresis curve under specific conditions. Table 7 displays the mechanical properties of various damper types at a natural frequency of 2 Hz. The downscaled damper, referenced in the study, utilized the newly discovered scale factor from the similitude law to accurately reflect the actual damper properties.

Table 7 Mechanical properties of damper types at specific condition

Parameter	Downscaled		
	Damper 1	Damper 2	Damper 3
Brand	APIDO	ESPADA	SKK
Exponent	1.0	1.0	1.0
Damping Coefficient, C, N.(s/m)	1219.32	1019.18	1028.3
Max. viscous force, N	186.8	132.3	127.63
Natural Frequency	2	2	2
Max. Stroke	±10mm	±10mm	±10mm

Damper 1 was observed to be stiffer than Damper 2 and Damper 3, which can be attributed to its higher damping coefficient and viscous force. These dampers were assumed to be linear when operating at a natural frequency of 1 Hz and above. However, if the natural frequency fell below 1 Hz, a non-linear damper was assumed based on observations of the hysteresis curve. Additionally, the maximum available stroke was measured at ±10 mm, which translates to ±80 mm in the prototype damper.

3.3 Displacement Response of Bare Frame DRCM and Structural Damage

Table 8 summarises the maximum displacement for each floor level (FL) and the inter-storey drift between floors at each SL of shaking. The overall maximum displacement of the DRCM at SL 2 is found to be larger than at SL 1. The unit displacement during the simulation is consistent at both SLs, measuring 3 mm/mm, but the frequency of shaking at SL 2 is 1 Hz higher than at SL 1. As a result, the DRCM exhibits more significant motion at SL 2.

Table 8 Inter-storey drift of bare frame at all SLs

	Inter-storey drift (mm)		
SL	FL 1	FL 2	FL 3
1	0.65	0.70	0.36
2	1.45	2.08	0.13
3	4.69	3.71	1.22
4	5.16	3.77	0.80
5	1.26	3.37	1.13
6	0.38	0.94	0.73
7	0.06	0.80	0.31
8	0.01	0.36	0.47
9	0.25	0.86	0.56
10	0.65	0.70	0.36
Avg.	1.54	1.84	0.63

Furthermore, the overall displacement or movement of the DRCM at SL 4 is greater than at SL 3, despite the shaking frequency remaining constant at 3 Hz. This observation is likely due to the more significant unit displacement of shaking at SL 4. A similar trend is observed in the results from SL 9 and SL 10: when either the shaking frequency or unit displacement is increased while keeping the other parameter constant, there is a corresponding increase in the maximum displacement observed in the system.

SL 5 serves as the intermediate level, where the intensity of shaking is increased to simulate more aggressive seismic activity. The maximum displacement on all floors decreases significantly at this SL compared to previous. The building behaviour shifts from large lateral movement to intense vibration from this SL onward. The DRCM is observed to have the highest inter-storey drift of 5.16 mm at SL 4, as highlighted in yellow. Additionally, the rooftop displacement of the bare frame DRCM is greater than

the ground displacement by about 10 mm at these SLs.

The results indicate that the higher floors of the DRCM experience the largest displacement amplitudes compared to the lower floors when the shaking displacement is moderate with low aggressiveness. This disparity can result in significant damage or even collapse of the upper floors during an earthquake.

Figure **8** 8 shows the mode shape of the bare frame DRCM at each SL, depicting the deformed shape of the building. From SL 1 to 4, the mode shape exhibits a single curvature, indicating that the building experiences translational motion and sways in one direction only, with minimal torsional or rotational motion. As the shaking SL increases to SL 8, the mode shape transitions to a double curvature, which signifies the presence of two different curvatures in different directions.

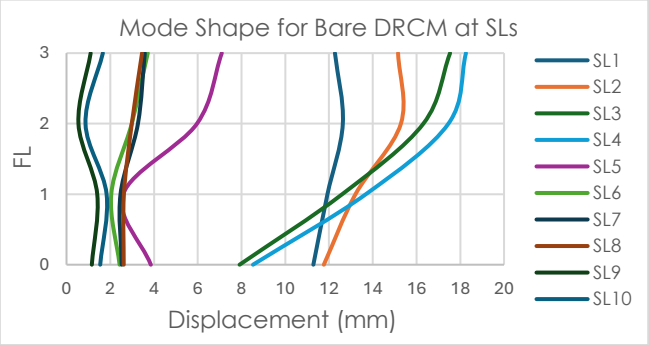

Figure 8 Mode shape for bare frame DRCM at different SLs

At SL 9 and 10, the mode shape evolves into a double S curvature. This type of mode shape occurs when the maximum displacement of the second floor is lower than that of the first and third floors during shaking.

Throughout the STA conducted on the bare frame DRCM, damage was observed, with cracking found on the concrete surface. The simulated ground motion caused the DRCM to oscillate and rotate, inducing forces and moments in the structural elements. When the internal forces exceed the yield strength of a member, plastic bending occurs, leading to plastic deformation. A plastic hinge forms at the location of the maximum bending moment, enhancing the DRCM's flexibility by allowing free rotation. This formation enables the structural member to deform plastically without resulting in catastrophic failure, serving as a type of energy dissipation device and improving the building's seismic performance.

Generally, the formation of a plastic hinge in a reinforced concrete member does not cause concrete cracks, as it occurs primarily in the steel reinforcement rather than the concrete itself. However, plastic deformation may lead to spalling or cracking of the concrete cover under certain conditions. This can happen when the bond strength between the reinforcement and the surrounding concrete is weaker than the tension in the reinforcement. Insufficient steel reinforcement or inadequate concrete cover may also contribute to concrete spalling and cracking.

In a 1-bay frame DRCM, plastic hinges typically form at the beam-to-column connections where the maximum bending moment occurs. The beams are designed with appropriate plastic hinges to dissipate seismic energy without collapsing, while the columns are designed to remain elastic and stabilise the DRCM during an earthquake.

Figure 9 (a) and (b) show the concrete cracking observed on the first-floor beams of the DRCM, starting from SL 3 of shaking. The plastic hinges formed allow the beam-column joints of the first floor to rotate in conjunction with the lower columns. Figure 9(c) shows the plastic hinges observed at the top of the second-floor columns starting from SL 4, while Figure 9(d) illustrates the formation of plastic hinges at the top of the first-floor column after SL 5 of the earthquake simulation. The plastic deformation of the structural members enables the DRCM to absorb more energy before collapsing during seismic events.

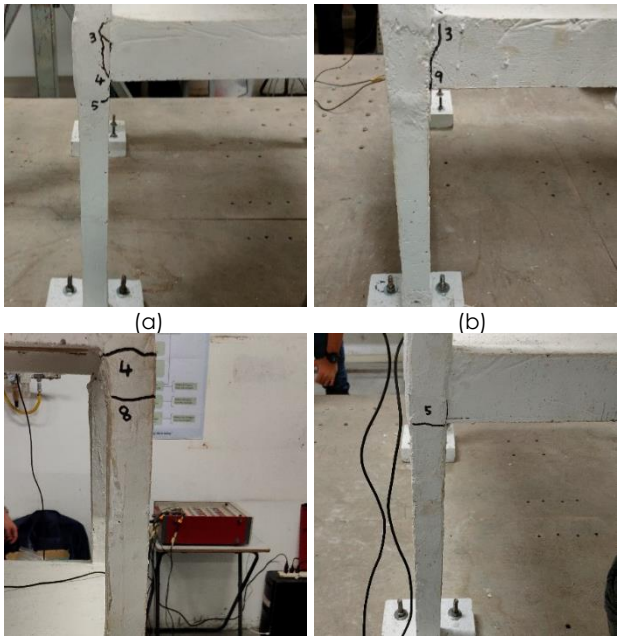

Figure 9 Concrete cracking on (a) & (b) first floor beams (c) second floor column (d) first floor column

3.4 Displacement Response for DRCM with and without Damper

Figure 10 shows the mode shape comparison between the DRCMs at SL 1 and SL 2 of shaking. When comparing the mode shapes of the bare frame DRCM with those of the DRCMs equipped with dampers, no significant improvement in lateral displacement reduction is observed in the damper-equipped DRCMs at SL 1. The bare frame DRCM exhibits a single

curvature mode shape at this SL, while all other DRCMs display a double curvature mode shape, which is preferable in seismic design. Double curvature mode shapes allow the DRCM to absorb more earthquake energy and undergo greater deformation before ultimate failure, as they are more ductile than single curvature mode shapes. Moreover, the experiment setup of SL1 and 2 was similar to that in [17], with the key difference being the type of dampers used. In the previous research, dampers with a backbone curve effect were selected, whereas in the current research, dampers were used without this effect. As a result, the displacement drift in SL1 was reduced by approximately 25%, while SL2 showed a reduction of about 30%. This suggests that the backbone curve leads to a reversal effect when comparing both studies.

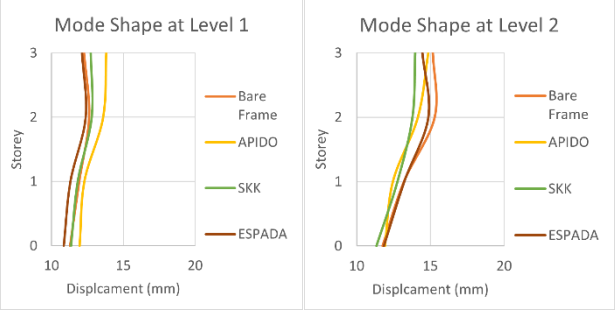

(a) (b)

Figure 10 Mode shape for DRCMs at (a) SL 1 (b) SL 2

At SL 2 of the earthquake simulation, only the DRCM with APIDO dampers shows a double curvature mode shape. All DRCMs with dampers demonstrate a slight reduction in rooftop displacement at this SL. These results indicate that the damping system can marginally reduce the dynamic response of the DRCM when the shaking displacement is large, but the aggressiveness is low. Under significant lateral ground motion, the entire DRCM tends to sway in the direction of the shaking. The inverted V shape of the braces provides additional stiffness and strength, enhancing the structural resistance to lateral loads. Thus, the inverted V diagonal braced-damper system effectively reduces the DRCM's response to ground movement and restrains the building's sway during an earthquake.

During the STA, with moderate displacement and low aggressiveness, the lateral movement of the DRCM equipped with dampers is smaller than that of the bare frame DRCM at SL 3 and 4, as shown in Figure 11. The inverted V diagonal braced-damper system effectively reduces the dynamic response of the building, regardless of the brand of viscous dampers used. Additionally, the inter-storey drift of the DRCM decreases compared to the bare frame DRCM, indicating that the viscous dampers successfully absorb some of the energy induced by the earthquake. This energy dissipation device minimizes the pseudo dynamic load acting on the building, thereby enhancing its seismic performance.

Based on the experimental data obtained from SL 3 and 4, the DRCM with the APIDO damping system demonstrates the best performance among all tested DRCMs, showing not only the least rooftop displacement but also the least inter-storey drift at both SLs. At SL 3, a double S curvature mode shape is observed in the DRCM with APIDO dampers. This mode shape is preferred during an earthquake, as it provides greater stability to the building compared to a single curvature mode shape. The double S curvature mode shape behaves similarly to a double curvature mode shape, distributing lateral loads more evenly throughout the DRCM. Consequently, the earthquake loads and stresses are less concentrated on any single floor, reducing the risk of structural collapse.

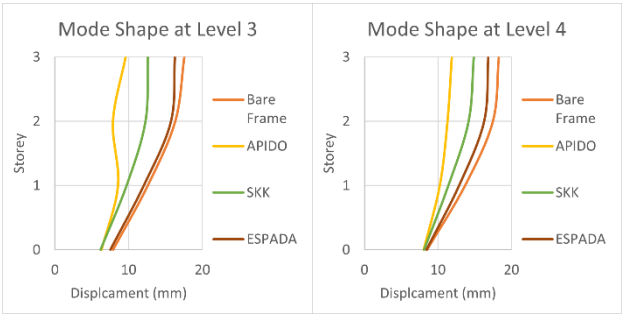

(a) (b)

Figure 11 Mode shape for DRCMs at (a) SL 3 (b) SL 4

Figure 12(a) shows the mode shapes of the testing DRCM at SL 5, characterized by moderate displacement and high aggressiveness of earthquake motion. Based on the mode shapes obtained from the STA, the bare frame DRCM appears to perform better than the DRCM equipped with a damping system at this SL. The DRCMs with ESPADA dampers and the bare frame DRCM exhibit similar behaviour, as their mode shapes closely resemble each other. Conversely, the DRCM with APIDO dampers demonstrates the poorest performance, showing a straight mode shape with significant rooftop displacement. During the earthquake simulation, this DRCM sways heavily in one direction, which could result in structural damage and potentially lead to collapse. At this SL, the damping system proves ineffective, as it fails to dissipate seismic energy and reduce the lateral movement of the DRCM caused by ground motion. As the shaking progresses to the next SL, the ground movement transitions from moderate displacement to short displacement. The mode shapes at this SL indicate a significant improvement in the dynamic response of the DRCMs with damping systems compared to the bare frame DRCM. Figure 12(b) shows a notable reduction in horizontal movement for the DRCMs with damping systems at SL 6 of shaking. Therefore, the inverted V diagonal braced-damper system

effectively absorbs seismic energy and reduces the amplitude of building vibrations at this SL, regardless of the brand. The movement of the viscous dampers' pistons within the compressible fluid generates a resistance force that opposes the building's motion, ultimately enhancing structural behaviour during seismic events.

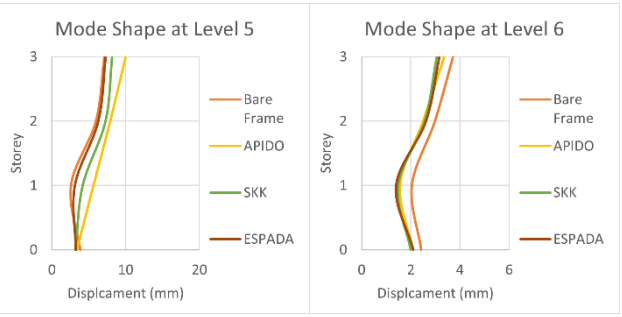

(a) (b)

Figure 12 Mode shape for DRCMs at (a) SL 5 (b) SL 6

In this study, SL 7 and 8 simulated ground motion characterized by short displacement and high aggressiveness. At SL 7, the bare frame DRCM exhibits a double curvature mode shape, demonstrating the largest displacement among the testing DRCMs, as shown in Figure 13(a). This observation indicates that the DRCMs equipped with dampers have better seismic performance compared to the bare frame DRCM. The damping systems effectively absorb seismic energy, resulting in a reduced overall response of the DRCMs during shaking. Although the DRCMs with different brands of viscous dampers experience similar ground movement, their rooftop displacements vary, highlighting differences in the effectiveness of these dampers in reducing rooftop displacement. The DRCM with SKK dampers outperforms those with APIDO and ESPADA dampers, as it demonstrates a double S curvature mode shape at SL 7. This behaviour allows SKK dampers to distribute earthquake loads uniformly across all floors, preventing load concentration on any single floor that could lead to structural failure, while the other dampers do not achieve a double curvature mode shape at this SL.

Figure 13(b) shows that at SL 8, the DRCMs with SKK dampers and ESPADA dampers behave similarly. Both DRCMs exhibit identical mode shapes, ground movement, and rooftop displacement. However, the APIDO dampers show relatively low effectiveness in enhancing the seismic performance of the building at this SL, as they provide only a slight reduction in displacement on the lower floors. Conversely, the amplitude of vibrations observed on the top floor is greater than in the other DRCMs. Both the DRCMs with APIDO dampers and the bare frame DRCM exhibit single curvature mode shapes, which are undesirable in seismic design due to load concentration issues. While the ground movement of the DRCM with APIDO dampers is smaller than that of the bare frame DRCM, its rooftop displacement is larger, indicating that the damping system fails to effectively dissipate seismic energy.

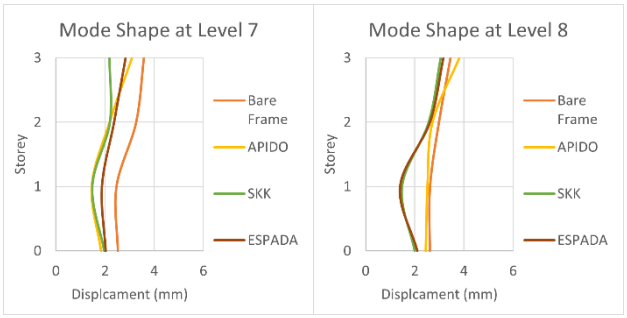

(a) (b)

Figure 13 Mode shape for DRCMs at (a) SL 7 (b) SL 8.

Figure 14 illustrates that the mode shapes of all DRCMs obtained at SL 9 and 10 exhibit a double S curvature, except for the DRCM with SKK dampers at SL 9, which presents a straight mode shape. The difference in ground and rooftop displacement for the DRCM with SKK dampers is less than 0.2 mm, indicating minimal inter-storey drift. This minimal relative translational displacement between two consecutive floors suggests that lateral forces from earthquakes are distributed efficiently across the different floors, thereby preventing excessive deformation and structural damage.

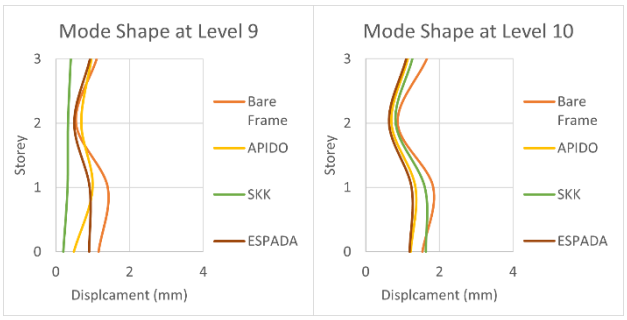

(a) (b)

Figure 14 Mode shape for DRCMs at (a) SL 9 (b) SL 10

Among the SLs, the damped frames in SL9 experienced the most significant storey drift reduction, with APIDO achieving a 12.47% reduction, SKK 63.44%, and ESPADA 16.27% compared to the bare frame. Figure 15 shows the hysteresis curves measurements of the roof top displacement against ground accelerations of SL9 for all frames. A clear observation is that the bare frame exhibits the largest curve among all cases, indicating its low stiffness of 3116.18 N/m, as shown in Table 9. In contrast, APIDO, ESPADA, and SKK frames figured in smaller hysteresis curves, demonstrating the high efficiency of the dampers in protecting structure from deformation and formation of plastic hinge during the SL9 simulation. Notably, the SKK damper shows the greatest potential for resisting high-intensity seismic simulations, as its hysteresis curve is the smallest among the damped frames. However,

it is concluded that the bare frame had already reached its plastic limit stage without collapsing during the SL4 and SL5 simulations, which may explain its larger hysteresis curve size.

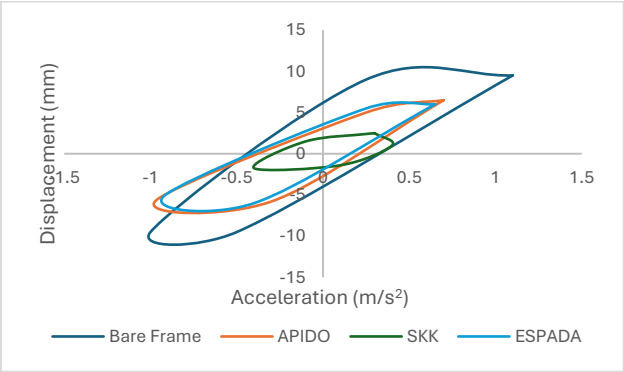

Figure 15 Hysteresis curve of SL 9.

Table 9 Frame stiffness

Frame Type	Stiffness, k (N/m)
Bare	3116.18
APIDO	3533.81
SKK	8569.50
ESPADA	3725.87

At SL 10, the DRCMs with dampers demonstrate significant improvements in reducing rooftop displacement, indicating less intense vibrations compared to the bare frame DRCM. Consequently, the DRCMs are more stable with the presence of damping systems, as the braced dampers effectively absorb seismic energy through tension and compression forces, thus reducing the dynamic response of the DRCM during an earthquake. Despite the high shaking frequency, the overall amplitude of lateral movement in the DRCMs remains below 2 mm, resulting in intense vibrations without substantial lateral displacement.

Table 10 presents the percentage reduction in rooftop displacement for each damper across all SLs in the STA. The results indicate a general improvement in reducing rooftop displacement throughout most of the earthquake simulations. However, SL 5 represents the worst-case scenario, where all dampers fail to effectively mitigate the dynamic response of the building. At this intermediate level, the DRCM transitions from significant lateral movement to intense vibration when subjected to the simulated pseudo-dynamic load.

Starting from SL 6, the rooftop displacements are consistently below 4 mm, which is minimal considering the height of the DRCM (1500 mm). The results show that the DRCM experiences horizontal movement when the shaking frequency is relatively low. Conversely, as the shaking intensifies, the DRCM begins to vibrate with smaller amplitudes.

Table 10 Summary rooftop displacement and reduction percentage of each damper at all SLs

Level	Intensity		Rooftop displacement (mm)				Reduction percentage (%)		
	Displacement	Aggressiveness	Bare frame	APIDO	SKK	ESPADA	APIDO	SKK	ESPADA
1	Large	Very low	12.27	13.82	12.73	12.12	-12.61	-3.72	1.21
2	Large	Low	15.16	14.86	13.97	14.45	1.98	7.83	4.69
3	Moderate	Low	17.53	9.57	12.61	16.25	45.43	28.08	7.32
4	Moderate	Low	18.26	11.88	14.85	16.86	34.91	18.66	7.68
5	Moderate	Aggressive	7.10	10.01	8.15	7.28	-41.05	-14.81	-2.60
6	Short	Aggressive	3.71	3.36	3.05	3.16	9.46	17.91	14.85
7	Short	Aggressive	3.58	3.09	2.18	2.83	13.58	39.11	20.78
8	Short	Aggressive	3.45	3.82	3.15	3.43	-10.49	8.91	0.79
9	Short	Very high	1.10	0.97	0.40	0.92	12.47	63.44	16.27
10	Short	Very high	1.66	1.14	1.27	1.10	31.16	23.71	33.70

4.0 CONCLUSION

This research concludes with findings from testing a bare frame DRCM and a DRCM equipped with three types of viscous dampers: APIDO, SKK, and ESPADA, under ten SLs of earthquake simulation with varying intensities. The seismic behaviour of the DRCMs—both with and without dampers—was evaluated in terms of inter-storey drift and mode shape.

One notable observation is that the APIDO damper demonstrated the highest effectiveness in dissipating seismic energy during low-aggressiveness shaking with moderate displacement, outperforming the other dampers. Conversely, the SKK damper was found to enhance seismic behaviour most effectively during high-frequency, short-distance simulated earthquake motions. The ESPADA damper performed moderately across most conditions, regardless of shaking intensity.

As the shaking frequency and unit displacement change, the behaviour of the DRCMs varied, resulting in different mode shapes. Double S curvature and

double curvature mode shapes are preferable in seismic design as they provide greater stability and resistance to lateral loads. These mode shapes distribute seismic forces more evenly throughout the DRCM, reducing undesirable load concentration on any single floor. This improved energy absorption and deformation capacity before failure can help prevent sudden building collapse, thereby averting catastrophic consequences.

Lastly, a key finding of this research is that the DRCM exhibited smaller inter-storey drift under various intensities of ground movement when equipped with the APIDO, SKK, and ESPADA viscous dampers. The STA results indicate that these dampers can achieve maximum reductions of 45%, 63%, and 34% in rooftop displacement, respectively. Based on the key findings, the placement of the inverted V diagonal damper system was effective and consistent during S-waves. However, the stiffest APIDO damper showed the least effectiveness on average during S-waves, though it demonstrated effective performance in certain scenarios during P-waves, albeit inconsistently. Among the dampers, the moderately stiff SKK damper with damping coefficient of 1028.3 Ns/m yielded the most optimal and consistent performance overall that suitable to apply in low-rise type of building. Overall, the selection of viscous damping systems is crucial neither too stiff nor too soft or not to prevent in reversal effect. A balanced viscous damping systems significantly enhances the seismic resistance of the DRCM, as evidenced by the general improvements in its displacement response under consistent pseudo dynamic load.

Further research is recommended to explore how machine learning models may be used to forecast seismic response and adjust the damper's damping constant to enhance seismic response, including seismic energy dissipation.

Acknowledgement

This author expresses gratitude to the Universiti Tunku Abdul Rahman IPSR Research Grant for supporting Project No. IPSR/RMC/UTARRF/2022-C1/Y05 and Project No. IPSR/RMC/UTARRF/2023-C2/Y02.

Conflicts of Interest

The authors declare that there is no conflict of interest regarding the publication of this paper.

References

[1] Kocoglu, E., Demir, F.B., Oteles, U.U., and Ozeren, E. 2023. Post-Earthquake Trauma Levels of University Students Evaluation: Example of 6 February Kahramanmaras Earthquake. *Higher Education Studies*. 13(2): 121. https://doi.org/10.5539/hes.v13n2p121.

[2] Louis, J. 2015. Mercy Malaysia's Response to The Sabah Earthquake.

[3] Zhang, Y., Xu, Y., Du, P., Li, W., Chen, L., and Tian, Q. 2020. The Volume Calculation Method of Rock Collapses and Loess Landslides Triggered by the 1556 AD Huaxian M 8 1/2 Earthquake in Shaanxi Province, China. *Earthquake Research in China*. https://doi.org/10.19743/j.cnki.0891-4176.202004001.

[4] Feng, X., Ma, J., Zhou, Y., England, P., Parsons, B., Rizza, M. A., and Walker, R. T. 2020. Geomorphology and Paleoseismology of the Weinan Fault, Shaanxi, Central China, and the Source of the 1556 Huaxian Earthquake. *Journal of Geophysical Research: Solid Earth*. 125. https://doi.org/10.1029/2019JB017848.

[5] Tongkul, F. 2021. An Overview of Earthquake Science in Malaysia. *ASM Science Journal*. 14: 1–12. https://doi.org/10.32802/asmscj.2020.440.

[6] Simone, P., Nicholas, R., Amy, G., and Felix, T. 2019. Deciphering the Fate of Plunging Tectonic Plates in Borneo. *Eos Transactions American Geophysical Union*.

[7] Abd Razak, J. A., Rambat, S., Che Ros, F., Shi, Z., and Mazlan, S. A. 2021. Seismic Vulnerability Assessment in Ranau, Sabah, Using Two Different Models. *ISPRS International Journal of Geoinformation*. 10(5): 271. https://doi.org/10.3390/ijgi10050271.

[8] Rosly, M. H., Mohamad, H. M., Bolong, N., and Harith, N. S. H. 2022. An Overview: Relationship of Geological Condition and Rainfall with Landslide Events at East Malaysia. *Trends in Sciences*. 19: 3464. https://doi.org/10.48048/tis.2022.3464.

[9] USGS, EMSC. 2024. Malaysia Earthquake Report. *Earthquakelist.Org*. https://earthquakelist.org/malaysia/#latest-earthquakes-mag-6-distance-smart.

[10] Dayak Daily. 2023. Expert Claims Malaysia Already Inside Pacific Ring of Fire as Sarawak, Sabah Also at Risk of Earthquakes. *Dayak Daily*. https://dayakdaily.com/expert-claims-malaysia-already-inside-pacific-ring-of-fire-as-sarawak-sabah-also-at-risk-of-earthquakes/

[11] Chong, W. K., Wong, J. Y., Yip, C. C., Ling, L., & Amran, M. 2025. Evaluating Viscous Damping for Seismic Energy Dissipation in Downscaled Concrete Structures Under Consistent Earthquake Loadings. *Structures*. 78: 109313. https://doi.org/10.1016/j.istruc.2025.109313.

[12] Wu, X., Guo, W., Hu, P., Bu, D., Xie, X., and Hu, Y. 2020. Seismic Performance Evaluation of Building-Damper System under Near-Fault Earthquake. *Shock and Vibration*. https://doi.org/10.1155/2020/2763709.

[13] Tatar, A., Baker, A. M., and Dowden, D. M. 2023. A Generalized Method for Numerical Modeling of Seismically Resilient Friction Dampers Using Flat Slider Bearing Element. *Engineering Structures*. 275: 115248. https://doi.org/10.1016/j.engstruct.2022.115248.

[14] Riaz, R. D., Malik, U. J., Shah, M. U., Usman, M., and Najam, F. A. 2023. Enhancing Seismic Resilience of Existing Reinforced Concrete Building Using Non-Linear Viscous Dampers: A Comparative Study. *Actuators*. 12(4): 175. https://doi.org/10.3390/act12040175.

[15] Qi, L., Xue, J., Sui, Y., and Wu, Z. 2021. Smart Retrofitting of Irregular Steel Joints in Traditional Chinese Buildings by Viscous Dampers. *Engineering Structures*. 228. https://doi.org/10.1016/j.engstruct.2020.111526.

[16] Li, Z. and Shu, G. 2019. Optimal Placement of Metallic Dampers for Seismic Upgrading of Multistory Buildings Based on a Cost-Effectiveness Criterion Using Genetic Algorithm. *The Structural Design of Tall and Special Buildings.* 28(6). https://doi.org/10.1002/tal.1595

[17] Yip, C. C., Wong, J. Y., Amran, M., Fediuk, R., and Vatin, N. I. 2022. Reliability Analysis of Reinforced Concrete Structure with Shock Absorber Damper under Pseudo-Dynamic Loads. *Materials*. 15(7). https://doi.org/10.3390/ma15072688.

[18] Latifee, E. R. 2020. Earthquake and Seismic Analysis-of Buildings-The Difficulties Examined. *Journal of Recent*

Activities in Infrastructure Science. 5: 26–37. https://doi.org/10.46610/JoRAIS.2020.v05i03.004.
[19] U.S.NRC. 2003. Selection of the Design Earthquake Ground Motion Reference Probability. United States Nuclear Regulatory Commission.
[20] Casaburo, A., Petrone, G., Franco, F., and De Rosa, S. 2019. A Review of Similitude Methods for Structural Engineering. *Applied Mechanics Reviews*. 71. https://doi.org/10.1115/1.4043787.
[21] Yip, C. C., Marsono, A. K., Wong, J.Y., and Lee, S. C. 2017. Seismic Performance of Scaled IBS Block Column for Static Nonlinear Monotonic Pushover Experimental Analysis. *Jurnal Teknologi (Sciences & Engineering)*. 80(1). https://doi.org/10.11113/jt.v80.10799.
[22] Pang, J. W., Yip, C. C., Ling, L., Wong, J. Y., Lam, F. S., and Wong, C. F. 2024. Finite Element Simulation of Low-Rise School Building Model with Seismic Loads Input. *Jurnal Teknologi (Sciences & Engineering)*. 86: 141–152. https://doi.org/10.11113/jurnalteknologi.v86.22019.
[23] Lee, S. C., and Ma, C. K. 2021. Time History Shaking Table Test and Seismic Performance Analysis of Industrialised Building System (IBS) Block House Subsystems. *Journal of Building Engineering*. 34. https://doi.org/10.1016/j.jobe.2020.101906.
[24] Ramu, M., and Prabhu, R.V. 2013. Establishment of Structural Similitude for Elastic Models and Validation of Scaling Laws. *KSCE Journal of Civil Engineering*. 17(1): 139–144. https://doi.org/10.1007/s12205-013-1216-x.
[25] Kenan, H., and Azeloğlu, O. 2020. Design of Scaled Down Model of a Tower Crane Mast by Using Similitude Theory. *Engineering Structures*. 220. https://doi.org/10.1016/j.engstruct.2020.110985.
[26] Boron, P., Chelmecki, J., Dulinska, J. M., Jurkowska, N., Ratajewicz, B., Stecz, P., and Tatara, T. 2023. On the Possibility of Using 3D Printed Polymer Models for Modal Tests on Shaking Tables: Linking Material Properties Investigations, Field Experiments, Shaking Table Tests, and FEM Modeling. *Materials*. 16(4): 1471. https://doi.org/10.3390/ma16041471.
[27] Wang, T., Shao, J., Zhao, C., Liu, W., and Wang, Z. 2021. Shaking Table Test for Evaluating the Seismic Performance of Steel Frame Retrofitted by Buckling-Restrained Braces. *Shock and Vibration*. https://doi.org/10.1155/2021/6654201.
[28] Nama, M. Y., Salem, L. A., and Mosa, A. M. 2023. Simplified Analytical Model and Shaking Table Test Validation for Seismic Analysis of Piled Raft Foundation. *International Journal of Science and Business*. 22(1): 102–114. https://doi.org/10.58970/IJSB.2098.
[29] ASTM Standard 33. 2018. *Standard Specification for Concrete Aggregates ASTM International*.
[30] ASTM Standard C150, 2012. *Standard Specification for Portland Cement., West Conshohocken: ASTM International.*
[31] Naghavi, M., Rahnavard, R., Thomas, R. J. and Malekinejad, M. 2019. Numerical Evaluation of the Hysteretic Behavior of Concentrically Braced Frames and Buckling Restrained Brace Frame Systems. *Journal of Building Engineering*. 22: 415–428. https://doi.org/10.1016/j.jobe.2018.12.023